Heuristic Dynamic Ramping Constraints for Demand Response of Processes with Internal Dynamics

Florian Joseph Baader [a,b,c 1], André Bardow [a,b] and Manuel Dahmen [a]

[a] Energy Systems Engineering (IEK-10), Forschungszentrum Jülich GmbH, 52425 Jülich, Germany

[b] Energy & Process Systems Engineering, ETH Zürich, Zürich 8092, Switzerland

[c] RWTH Aachen University, Aachen, 52062, Germany

Abstract

Simultaneous scheduling of production processes and their multi-energy systems could provide demand response. However, such scheduling results in nonlinear mixed-integer dynamic optimization problems, which are hard to solve in real time. The optimization problem can be simplified by dynamic ramping constraints (DRCs) that limit the rate of change of scheduling-relevant quantities instead of modeling nonlinear process dynamics. By employing piecewise affine limits, DRCs allow a mixed-integer linear programming (MILP) formulation. In this contribution, we present a heuristic parameterization of DRCs for processes with uncontrolled internal dynamics for which DRCs cannot be derived rigorously. First, the true ramping limits are derived as a function of all process states. Based on simulation experiments, DRCs are then parameterized to hold for all simulation points. We apply this heuristic approach to a distillation column, which can shift heat demand in time by varying its purity. This column is scheduled simultaneously with three energy system units. The simultaneous scheduling problem can be solved in less than 3 minutes, leading to a feasible operation on the full-order column model. Furthermore, the operational costs are reduced substantially compared to the steady-state benchmark.

Keywords

Demand response, Integration of scheduling and control, Mixed-integer dynamic optimization, Dynamic ramping

Introduction

Volatile electricity prices due to an increasing share of renewable electricity production render demand response (DR) attractive for energy-intensive production processes (Zhang and Grossmann, 2016). If processes can shift energy demand in time, flexible production scheduling reacting to electricity prices may reduce operational costs. However, many processes have scheduling-relevant dynamics. Incorporating nonlinear process dynamics leads to hard-to-solve scheduling optimization problems. Moreover, processes that do not only consume electricity but also heating or cooling need to be scheduled simultaneously with their local multi-energy supply system (Baader et al., 2022a). The discrete on/off decisions of energy system components add further combinatorial complexity and thus lead to mixed-integer dynamic optimization (MIDO) problems. At the same time, optimization must often be performed within 5-20 minutes for real-time scheduling (Harjunkoski et al., 2014). For this purpose, the process dynamics are often simplified by simple ramping constraints with constant limits (Adamson et al., 2017), data-driven surrogate models (Burnak et al., 2018), or low-order scale-bridging models (Du et al., 2015) in scheduling to avoid optimization with the full-order process model.

To bridge the gap between nonlinear process dynamics and simple ramping constraints, we introduced high-order dynamic ramping constraints (DRCs) (Baader et al., 2022b). Instead of modelling all process states $\mathbf{x}$ as a function of the inputs $\mathbf{u}$, DRCs only model the feasible space of the main scheduled variable ρ, e.g., the process production rate. The aim is to ensure that a set-point trajectory for the scheduled variable ρ, resulting from the optimization, can be realized by the closed-loop process, i.e., the process and its control. To this end, DRCs use an alternative coordinate system in which the process is linear, and the δ-th time derivative of the scheduled variable ρ is defined as ramping degree of freedom ν. The lower derivatives $\rho^{(\gamma)}$ ($\gamma = 1, ..., \delta - 1$) are ramping states. However, the new ramping-coordinate sys-

[1] Corresponding author. Email: fbaader@ethz.ch.

tem has nonlinear constraints even for originally linear input bounds ($\mathbf{u}^{\min} \leq \mathbf{u} \leq \mathbf{u}^{\max}$). If input bounds are violated, the underlying control cannot realize the set-point trajectory. Thus, the ramping degree of freedom $\nu = \rho^{(\delta)}$ and all lower time derivatives $\rho^{(\gamma)}$ need to be bounded by nonlinear functions of the scheduled variable ρ and lower time derivatives $\dot{\rho}, ..., \rho^{(\gamma-1)}$. The resulting DRCs read:

$$\begin{gathered} \rho^{(\delta)} = \nu \\ \dot{\rho}^{\min}(\rho) \leq \dot{\rho} \leq \dot{\rho}^{\max}(\rho) \\ (\rho^{(2)})^{\min}(\rho, \dot{\rho}) \leq \rho^{(2)} \leq (\rho^{(2)})^{\max}(\rho, \dot{\rho}) \\ \vdots \\ \nu^{\min}(\rho, \dot{\rho}, ..., \rho^{(\delta-1)}) \leq \nu \leq \nu^{\max}(\rho, , \dot{\rho}, ..., \rho^{(\delta-1)}) \end{gathered} \tag{1}$$

The nonlinear functions $(\rho^{(\gamma)})^{\min}$, $(\rho^{(\gamma)})^{\max}$ can be derived rigorously for the special case of flat processes (Baader et al., 2022b).

DRCs have the advantage compared to nonlinear process models that approximating the nonlinear functions $(\rho^{(\gamma)})^{\min}$, $(\rho^{(\gamma)})^{\max}$ conservatively by piecewise affine (PWA) functions, gives a mixed-integer linear programming (MILP) formulation. Solving the mixed-integer linear program leads to feasible operation on the original nonlinear model and is sufficiently fast for real-time application (Baader et al., 2022b). Due to their ability to capture high-order dynamics and non-constant ramping limits, DRCs can capture more flexibility than static first-order ramping constraints. However, the rigorous derivation of DRCs is restricted to flat process models (Baader et al., 2022b). For non-flat processes, uncontrolled internal states require ramping limits that are functions of all process states, not only of the scheduled variable ρ and its derivatives.

The present paper presents a heuristic extension of dynamic ramping constraints for non-flat processes with uncontrolled internal states. First, we introduce a distillation column with variable purity ρ as a motivating example. We show that ramping limits can be derived as functions of all process states but not as functions of the purity ρ only due to uncontrolled internal states. Then, we present a simulation-based heuristic to parameterize DRCs that depend on the purity ρ only. Based on these DRCs, we perform a demand response case study scheduling the operation of the distillation column simultaneously with two combined heat and power plants (CHPs) and an electricity-driven boiler. Finally, we conclude the paper.

Motivating Example: Distillation Column

We consider a generic model of a binary distillation column based on Skogestad and Morari (1988) together with a liquid flow model from Skogestad et al. (1990). In our previous work, we considered the same column and varied its purity ρ with a simple linear scale-bridging model tuned in simulations (Baader et al., 2022a). In the present contribution, we derive dynamic ramping constraints for the purity of the column. We assume that the purity ρ can be varied within bounds $\rho^{\min}$, $\rho^{\max}$, as long as the nominal purity ρ^{nom} is reached on average over the time horizon of one day. By varying the purity, heating demand can be shifted in time. We couple the vapor mole fraction of the light component entering the total condenser Y_D with the purity ρ, and the liquid mole fraction in the bottom flow X_B with $1-\rho$. Note that this coupling $Y_D = 1 - X_B$ is possible as the column has a 50/50 split and the feed flow has a mole fraction of $X_F = 0.5$. A more general coupling is discussed in Baader et al. (2022a). We assume that the feed flow F is fixed by an upstream process, and the control inputs $\mathbf{u}$ are the four flow rates: reflux L, boilup V, distillate flow D, and bottom flow B. Apart from the mole fractions Y_D and X_B, the controlled outputs $\mathbf{y}$ are the condenser hold-up M_D and the reboiler hold-up M_B, which must be maintained at their respective nominal values M_D^{nom} and M_B^{nom}, irrespective of the current purity ρ, to avoid depletion. Thus, the set-points for all four outputs $\mathbf{y}$ are specified as a function $\boldsymbol{\pi}(\rho)$ of the purity ρ, only. Moreover, the output vector $\mathbf{y}$ can be given as a function of the states $\mathbf{x}$,

$$\mathbf{y}(\mathbf{x}) = \begin{pmatrix} \frac{\alpha X_N}{1+(\alpha-1)X_N} (= Y_D) \\ X_B \\ M_D \\ M_B \end{pmatrix} \stackrel{!}{=} \boldsymbol{\pi}(\rho) = \begin{pmatrix} \rho \\ 1-\rho \\ M_D^{nom} \\ M_B^{nom} \end{pmatrix}, \tag{2}$$

where X_N is the liquid mole fraction in the tray below the condenser, $N = 40$ is the number of trays, and α is the constant relative volatility. In total, the distillation column model has $n = 2N + 2 = 82$ differential states x, i.e., $N+1$ liquid mole fractions X_k, and $N+1$ liquid hold-ups M_k. The model can be written in input-affine control normal form

$$\dot{\mathbf{x}} = \mathbf{f}_1(\mathbf{x}) + \mathbf{f}_2(\mathbf{x})\mathbf{u}, \tag{3}$$

with nonlinear functions $\mathbf{f}_1 \colon \mathbb{R}^n \to \mathbb{R}^n$ and $\mathbf{f}_2 \colon \mathbb{R}^n \to \mathbb{R}^{4\times n}$.

In the following sections, we discuss the derivation of ramping limits for the purity ρ as functions of all states $\mathbf{x}$ and subsequently present a simulation-based heuristic to model the ramping limits as functions of the purity ρ only.

True Ramping Limits

DRCs should limit the derivatives of the purity ρ such that an underlying control can realize the chosen set-point trajectory on the original nonlinear process model (3). To derive DRCs, we first need to analyze which derivatives of the controlled process outputs $\mathbf{y}$ depend on the process inputs $\mathbf{u}$. As the output vector $\mathbf{y}$ is coupled with the purity ρ, the dependency between $\mathbf{y}$ and $\mathbf{u}$ allows us to analyze how the bounds on $\mathbf{u}$ limit the derivatives of the purity ρ. In the motivating example, all 4 components of the output vector can be controlled with first-order dynamics as after one time differentiation at least one of the inputs $\mathbf{u} = (L, V, D, B)$ appears:

$$\begin{aligned} \dot{\mathbf{y}} &= \frac{\partial \mathbf{y}(\mathbf{x})}{\partial \mathbf{x}} \dot{\mathbf{x}} = \left(\frac{\partial Y_D}{\partial X_N} \dot{X}_N, \dot{X}_B, \dot{M}_D, \dot{M}_B \right)^T \\ &= \begin{pmatrix} \frac{\partial Y_D}{\partial X_N} \frac{1}{M_N} \left(L X_{N+1} + V Y_{N-1} - L_N X_N - V Y_N \right) \\ \frac{1}{M_B} (L_2 X_2 - V Y_B - B X_B) \\ V - D - L \\ L_2 - V - B \end{pmatrix}, \end{aligned} \tag{4}$$

$$\text{with } \frac{\partial Y_D}{\partial X_N} = \frac{\alpha}{1+(\alpha-1)X_N} - \frac{(\alpha-1)\alpha X_N}{(1+(\alpha-1)X_N)^2}$$

In Eq. (4), Y_k is the vapor mole fraction leaving tray k and a function of X_k. L_k is the liquid flow leaving tray k and a function of M_k. Setting the derivative of the outputs $\dot{\mathbf{y}}$ equal to the total time differential of $\boldsymbol{\pi}(\rho)$, Eq. (4) becomes

$$\frac{\partial \boldsymbol{\pi}(\rho)}{\partial \rho}\dot{\rho} = \boldsymbol{\alpha}(\mathbf{x}) + \boldsymbol{\beta}(\mathbf{x})\mathbf{u}, \tag{5}$$

with nonlinear functions $\boldsymbol{\alpha}$: $\mathbb{R}^n \to \mathbb{R}^4$ and $\boldsymbol{\beta}$: $\mathbb{R}^n \to \mathbb{R}^{4\times 4}$, where $n = 82$ is the number of states. The matrix $\boldsymbol{\beta}(\mathbf{x})$ is structurally invertible, and we find that it is, in fact, invertible for any state vector $\mathbf{x}$ that we study. Thus, from Eq. (5), the input vector $\mathbf{u}$ can be expressed as function of the states $\mathbf{x}$ and the first derivative of the purity $\dot{\rho}$:

$$\mathbf{u}(\mathbf{x}, \dot{\rho}) = \boldsymbol{\beta}^{-1}(\mathbf{x}) \left(\frac{\partial \boldsymbol{\pi}(\rho)}{\partial \rho}\dot{\rho} - \boldsymbol{\alpha}(\mathbf{x}) \right) \tag{6}$$

Note that applying the input vector $\mathbf{u}(\mathbf{x}, \dot{\rho})$ on the process constitutes an exact input-output linearization (Corriou, 2018). The total relative degree is 4, as all four outputs are differentiated once with respect to time to receive Eq. (4). Thus, 78 of the 82 states remain as uncontrolled internal states, namely the compositions $X_2, ...X_{N-1}$ and hold-ups $M_2, ..., M_{N-1}$. Exact input-output linearization is only applicable if the internal dynamics are asymptotically stable (Corriou, 2018). Here, we assume that the internal column dynamics are stable as we did not find any indication of unstable dynamics in our simulations.

Based on the above analysis, we conclude that the ramping degree of freedom ν is equal to the first derivative of the purity, $\dot{\rho}$, i.e., for a given state of the process $\mathbf{x}$, the ramping degree of freedom $\nu = \dot{\rho}$ can be chosen freely. Thus, first-order ramping ($\delta = 1$ in Eq. (1)) is appropriate. The input vector $\mathbf{u}$ to achieve this ramping rate can be calculated from Eq. (6). However, the resulting input vector $\mathbf{u}$ must be within its bounds $\mathbf{u}^{\min}$ and $\mathbf{u}^{\max}$. Consequently, ramping limits $\nu^{\min}, \nu^{\max}$ are needed. If the state vector $\mathbf{x}$ is known, the true ramping limits $\nu^{\min}_{\text{true}}(\mathbf{x}), \nu^{\max}_{\text{true}}(\mathbf{x})$ can be calculated: If any of the inputs u_i ($i \in \{1, ..., 4\}$) is specified, the 4×4 Equation system (5) can be solved for the three other inputs u_j ($j \in \{1, ..., 4\} \setminus \{i\}$) and the derivative of the purity $\dot{\rho}$. By inserting the bounds $u_i^{\min}$, and $u_i^{\max}$ for every of the four output components $i \in \{1, ..., 4\}$, we receive four upper ramping limits $\nu_i^{\max}(\mathbf{x})$ and four lower ramping limits $\nu_i^{\min}(\mathbf{x})$. The true ramping limits are given by the lowest upper limit, $\nu_i^{\max}(\mathbf{x})$, and the highest lower limit, $\nu_i^{\min}(\mathbf{x})$, as all four inputs need to be within bounds.

In the following, we simplify the first-order ramping limits to

$$\dot{\rho} = \nu, \text{ with } \nu^{\min}(\rho) \leq \nu \leq \nu^{\max}(\rho), \tag{7}$$

compare to Eq. (1), because this form is computationally cheap. As the uncontrolled internal states $X_2, ...X_{N-1}$ and $M_2, ..., M_{N-1}$ cannot be expressed as functions of purity ρ and ramping degree of freedom ν, we first study the ramping limits in steady state, as in steady state, the states $\mathbf{x}^{\text{steady}}$ depend on the purity ρ only. During transitions, the state vector deviates from $\mathbf{x}^{\text{steady}}(\rho)$, and therefore also the ramping limits differ from their steady-state limits. To illustrate this effect, we perform simulation experiments: Starting from the lower purity bound $\rho^{\min} = 0.85$, the purity is ramped up until the upper bound $\rho^{\max} = 0.95$ is reached. During the transition, the ramping speed is always set equal to the true ramping limit $\nu^{\max}_{\text{true}}(\mathbf{x})$, calculated from the current state vector $\mathbf{x}$, multiplied with a relative ramping rate ν_{rel} between zero and one. In the simulations, we study three relative ramping rates: $\nu_{rel} = 1$, $\nu_{rel} = 0.25$, $\nu_{rel} = 0.01$ (Figure 1). For $\nu_{rel} = 1$, the upper ramping limit $\nu^{\max}_{\text{true}}(\mathbf{x})$ quickly drops and even becomes negative for a certain amount of time such that after 3 min the purity has to be reduced again (bottom plot). Interestingly, the ramping with $\nu_{rel} = 0.25$ is not much slower compared to $\nu_{rel} = 1$. For instance, after 5 min, $\nu_{rel} = 1$ reaches $\rho = 0.906$ and $\nu_{rel} = 0.25$ reaches $\rho = 0.901$. The complete transitions take 32 min ($\nu_{rel} = 1$) and 42 min ($\nu_{rel} = 0.25$). On the other hand, for $\nu_{rel} = 0.01$, the transition is much slower (421 min), and the ramping limits are nearly identical to the steady-state ramping limits. This finding is explainable for stable internal dynamics: If the purity is ramped very slowly, the state vector and thus the ramping limits are nearly in steady state.

Robust Ramping Limits

The aim is to find ramping limits that only depend on the purity ρ (Eq. (7)) and, at the same time, cover as much flexibility as possible without violating the true ramping limits derived above. Accordingly, we want to choose a function for the upper ramping limit $\nu^{\max}(\rho)$ that is equal to or smaller than the true upper ramping limit $\nu^{\max}_{\text{true}}(\mathbf{x})$ for every state vector $\mathbf{x}$ that can occur for a given purity ρ. The following discussion focuses on the upper ramping limit to ease readability. The extension to the lower ramping limit $\nu^{\min}$ is straightforward. Formally, the function for the upper ramping limit would ideally by chosen by solving the semi-infinite optimization problem:

$$\max_{\mathbf{p}} \int_{\rho^{\min}}^{\rho^{\max}} \nu^{\max}(\rho, \mathbf{p}) d\rho \tag{8}$$

$$\text{s.t. } \nu^{\max}(\rho, \mathbf{p}) \leq \nu^{\max}_{\text{true}}(\mathbf{x}) \; \forall \mathbf{x} \in \mathcal{X}(\rho) \; \forall \rho \in [\rho^{\min}, \rho^{\max}],$$

where $\mathbf{p}$ are the parameters of the function $\nu^{\max}(\rho)$, which must be a linear or PWA function as we aim for an overall MILP formulation. The set $\mathcal{X}(\rho)$ consists of all state vectors $\mathbf{x}$ than can occur for a given purity ρ. The challenge is that this set $\mathcal{X}(\rho)$ is unknown. Moreover, the above-stated ramping experiments have shown that the set $\mathcal{X}(\rho)$ depends on the relative ramping rate ν_{rel}: If the purity ρ is ramped with a high speed, possible state vectors spread widely around the steady state; in contrary, if the purity ρ is ramped slowly, possible state vectors are close to the steady state. The following section presents a heuristic procedure to choose dynamic ramping limits.

Heuristic Parameterization

Our heuristic procedure is based on the observation that the deviation of the true ramping limits from the steady-state limits heavily depends on the relative ramping rate ν_{rel}. Thus, if we limit the relative ramping rate, the deviation from

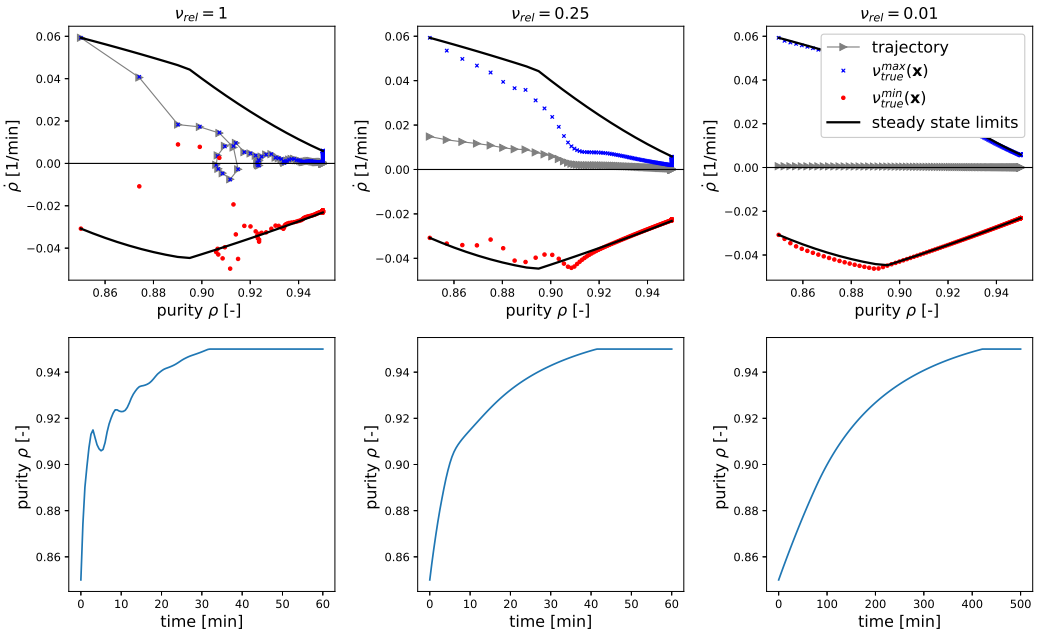

Figure 1: Numerical ramping experiments: The rate of change $\dot{\rho}$ is always set equal to the fraction ν_{rel} of the true maximum ramping limit $\nu_{true}^{max}(\mathbf{x})$ with $\nu_{rel} \in \{1, 0.25, 0.01\}$ (left to right). The upper plots show the trajectory of $\dot{\rho}$ over the purity ρ and the corresponding true and steady-state ramping limits. The lower plots show the purity ρ over time. Note that the x-axis extends to 500 min for $\nu_{rel} = 0.01$, while it only reaches 60 min for $\nu_{rel} = 0.1$ and $\nu_{rel} = 0.25$.

steady-state limits is limited as well. To study the maximum deviation from the steady-state ramping limits, we perform another round of numerical ramping experiments. More specifically, we first perform several ramping experiments as in Figure 1 for a fixed relative ramping rate ν_{rel}, which is a tuning factor. The ramping experiments result in a set of data points $\mathbb{J}$, where a data point j consists of purity ρ_j and state vector $\mathbf{x}_j$. Based on these data points, we determine the parameters $\mathbf{p}$ for the upper ramping limits $\nu^{\max}(\rho, \mathbf{p})$ by solving the optimization problem

$$\max_{\mathbf{p}} \sum_{j \in \mathbf{J}} \nu^{\max}(\rho_j, \mathbf{p}) \tag{9}$$
$$\text{s.t. } \nu^{\max}(\rho_j, \mathbf{p}) \leq \nu_{rel} \nu_{\text{true}}^{\max}(\mathbf{x}_j) \; \forall \mathbf{j} \in \mathbb{J},$$

which is a discretized variant of Problem (8).

The tuning factor ν_{rel} should neither be too large because then upper and lower ramping limits can overlap nor too small because then the ramping would be unreasonably slow. For our motivating example, we continue to study the three relative ramp rates $\nu_{rel} = 1$, $\nu_{rel} = 0.25$ and $\nu_{rel} = 0.01$. We split the purity range into 11 equally distributed points and ramp between every combination of points, leading to 110 experiments for each relative rate ν_{rel}. While upper and lower ramping limit overlap for $\nu_{rel} = 1$, the ramping limits stay close to their steady-state values for $\nu_{rel} = 0.01$ (Figure 2). Thus, our heuristic cannot be applied with $\nu_{rel} = 1$ but $\nu_{rel} = 0.01$ would be a feasible choice. However, $\nu_{rel} = 0.01$ would lead to an extremely conservative ramping. Here, $\nu_{rel} = 0.25$ offers a reasonable compromise as ramping is not much slower than with $\nu_{rel} = 1$ (Figure 1) but the true upper and lower ramping limits no longer overlap (Figure 2). Thus, we proceed with $\nu_{rel} = 0.25$ and choose piece-wise affine upper and lower ramping limits with two segments each and a breakpoint at the nominal purity $\rho^{\text{nom}} = 0.9$. These ramping limits are used in the following case study.

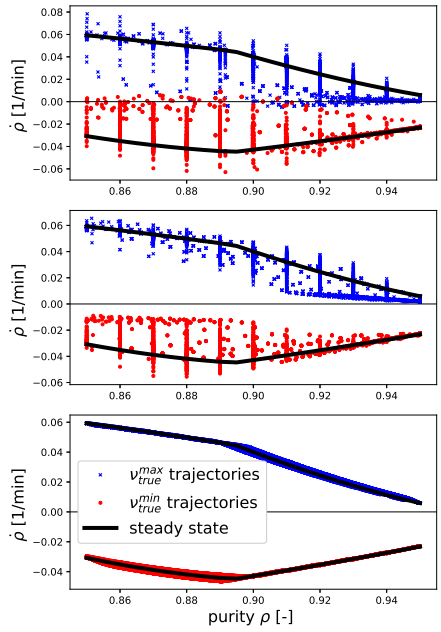

Figure 2: True ramping limits ν_{true}^{max}, ν_{true}^{min} observed during simulations with $\nu_{rel} = 1$ (top), $\nu_{rel} = 0.25$ (center), and $\nu_{rel} = 0.01$ (bottom).

Case Study

To study the developed DRCs in an application, we con-

sider a case study from our previous publication (Baader et al., 2022a), where the distillation column from the motivating example is supplied by an energy system consisting of two combined heat and power plants (CHPs) and an electricity-driven boiler (EB). Electricity can be bought from and sold to the grid at the current market price. Thus, time-varying prices provide an incentive to shift the heat demand of the column in time by varying the purity ρ.

First, a simultaneous scheduling optimization is performed in which the piecewise affine (PWA) dynamic ramping constraints limit the rate of change of the purity. The heat demand of the column is approximated by a data-driven model from our previous work (Baader et al., 2022a) that takes the purity ρ and the rate of change $\dot{\rho}$ as inputs. This heat demand model has an internal state to account for internal dynamics because, after a purity transition, the heat demand deviates from the steady-state heat demand for a certain amount of time. We assume that an approximate heat demand model is sufficient as small deviations between the predicted heat demand and the real heat demand can be compensated by the energy system units. The combined heat and power plants and the electricity-driven boiler have a part-load-dependent efficiency and a minimum part-load. The energy system is modeled by a standard MILP energy system model, see, e.g., Sass et al. (2020). The simultaneous scheduling optimization problem can be summarized as:

$$\begin{aligned} &\min \text{ Energy costs} \\ \text{s.t. } &\text{PWA dynamic ramping constraints (DRCs)} \\ &\text{PWA heat demand model} \\ &\text{MILP energy system model} \\ &\text{Production target} \end{aligned} \tag{10}$$

The production target is to reach the nominal purity on average over the one-day time horizon. As all models are linear or piecewise affine, discretization with collocation on finite elements leads to an overall MILP formulation that we solve with gurobi version 9.12 and an 1 % optimality gap.

Second, the resulting purity trajectory is used as set-point ρ_{SP} for a simulation of the controlled full-order distillation column model. The compositions Y_D and X_B are controlled by two PI-controllers that manipulate the flow rates L and V. Moreover, perfect level control is assumed for the controlled hold-ups M_D and M_B, i.e., the flow rates D and B are set such that these hold-ups stay at their nominal values. The simulation allows us to study the performance of our scheduling optimization result on the original nonlinear process model. We compare the resulting energy costs to a benchmark scenario in which the distillation column is operated in steady state and thus has a constant heat demand. Moreover, we benchmark the DRCs against the results from our previous paper (Baader et al., 2022a), where we used a linear scale-bridging model (SBM) instead of DRCs in Problem (10). The time constant of this SBM was tuned in closed-loop simulation experiments to achieve as-fast-as-possible linear dynamics.

Results

The simultaneous scheduling optimization Problem (10) is solved to 1 % optimality gap within 159 seconds, which is below the typical 5-20 minutes maximum runtime for scheduling applications (Harjunkoski et al., 2014). In the closed-loop simulation, the purity set-point ρ_{SP} from the scheduling optimization can be tracked well for both compositions Y_D and X_B (Figure 3). Both top and bottom product reach the nominal purity $\rho^{\text{nom}} = 0.9$ on average.

$$X_D^{average} = \frac{\int_{t=0h}^{t=24h} X_D D dt}{\int_{t=0h}^{t=24h} D dt} = 0.9004 > \rho^{nom} = 0.9 \tag{11}$$

$$X_B^{average} = \frac{\int_{t=0h}^{t=24h} X_B B dt}{\int_{t=0h}^{t=24h} B dt} = 0.0997 < 1 - \rho^{nom} = 0.1 \tag{12}$$

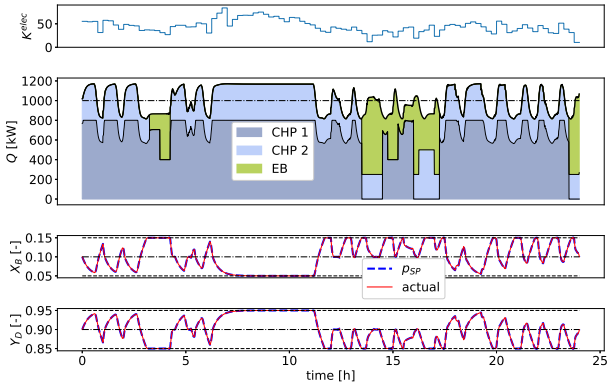

Figure 3: Resulting operation with dynamic ramping constraints. Top: Electricity price K^{elec} in €/MWh. Center: Heat demand Q of the column (bold black line) and nominal value (dashed-dotted line). The portions of the heat demand supplied by the two combined heat and power plants (CHP1 and CHP2) and the electricity-driven boiler (EB) are indicated with colors. Bottom: Actual values of bottom composition X_B and top composition Y_D together with their respective filtered set-points ρ_{SP} from scheduling optimization.

Compared to the steady-state benchmark, energy costs are reduced by 4.1 % through demand response. Both at times of high electricity prices and at times of low electricity prices, the distillation column operates at a high heat demand. However, while at times of high electricity prices, the high heat demand leads to high electricity production by the combined heat and power plants with the electricity being sold to the grid, at times of low prices, the electricity-driven boiler operates close to its maximum load (Figure 3). At times of medium prices, the column is operated with low heat demand.

With the SBM from our previous work (Baader et al., 2022a), we received a slightly higher cost reduction of 4.3 % as we applied a more aggressive tuning. As a result, the control inputs V and L saturated at their bounds several times. Still, in our simulations, this saturation does not lead to any problems, and thus the SBM reaches a better overall performance. With the new DRCs, the control inputs keep distance to their bounds, as shown for the case of V in Figure 4. Thus, the heuristic parameterization applied here introduces some conservatism. While this conservatism leads to slightly smaller cost reductions, it might be preferable from a practical point of view because when the inputs are saturated, the

underlying control can no longer react to disturbances.

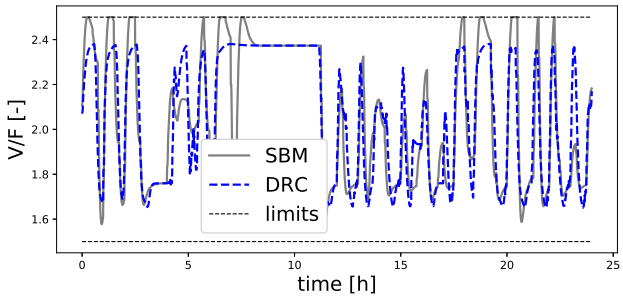

Figure 4: Boilup rate V normalized to the feed F for scheduling optimization with scale-bridging model (SBM) from Baader et al. (2022a) and the newly developed dynamic ramping constraints (DRCs).

Conclusions

Nonlinear process dynamics make scheduling optimization challenging, especially if processes need to be scheduled simultaneously with their multi-energy systems that introduce discrete decisions. Thus, simplified process representations are needed to enable real-time scheduling optimization. In this paper, we extend our dynamic ramping constraint (DRC) approach for the case of processes with uncontrolled internal dynamics. To this end, the ramping limits are derived from the full-order process model as a function of all process states and then studied in simulation experiments to allow a heuristic parameterization of the DRCs. For the distillation column example with variable purity, the DRCs lead to feasible operation on the full-order process model. At the same time, optimization is fast enough for real-time scheduling and leads to substantial cost reduction through demand response compared to a steady-state operation benchmark. Studying the resulting control inputs shows that the heuristic parameterization leads to a slightly conservative operation.

In the future, it should be further investigated to which class of processes the presented heuristic can be applied. One requirement is that the process is exact input-output linearizable with stable internal dynamics (compare to the remark after Eq. (6)). In general, the output components are controlled with dynamics of different orders, and the input bounds can give ramping limits on multiple derivatives. For instance, one input could give ramping limits on the first derivative $\dot{\rho}$, and another input could give ramping limits on the second derivative $\rho^{(2)}$. Then, generating simulation data for Problem (9) is more challenging, as not only does the acceleration $\rho^{(2)}$ has to be within bounds, but also the speed $\dot{\rho}$. Small accelerations $\rho^{(2)}$ might be a straightforward option here but carry the risk of poor performance due to an overly conservative parameterization of the DRCs. Hence, a more sophisticated procedure to generate simulation data might be needed.

Overall, the promising results from our case study motivate future research in dynamic ramping constraints.

Acknowledgement: FB, AB, and MD received funding from the Helmholtz Association of German Research Centres. FB and AB received financial support from the Swiss Federal Office of Energy through the SWEET PATHFNDR Project.

References

Adamson, R., M. Hobbs, A. Silcock, and M. J. Willis (2017). Integrated real-time production scheduling of a multiple cryogenic air separation unit and compressor plant. *Computers & Chemical Engineering 104*, 25–37.

Baader, F. J., A. Bardow, and M. Dahmen (2022a). Simultaneous mixed-integer dynamic scheduling of processes and their energy systems. *AIChE Journal e17741*.

Baader, F. J., P. Althaus, A. Bardow, and M. Dahmen (2022b). Demand Response for Flat Nonlinear MIMO Processes using Dynamic Ramping Constraints. *arXiv:2205.14598v2*.

Burnak, B., J. Katz, N. A. Diangelakis, and E. N. Pistikopoulos (2018). Simultaneous process scheduling and control: A multiparametric programming-based approach. *Industrial & Engineering Chemistry Research 57*(11), 3963–3976.

Corriou, J.-P. (2018). *Process control: Theory and applications* (Second edition ed.). Cham, Switzerland: Springer.

Du, J., J. Park, I. Harjunkoski, and M. Baldea (2015). A time scale-bridging approach for integrating production scheduling and process control. *Computers & Chemical Engineering 79*, 59–69.

Harjunkoski, I., C. T. Maravelias, P. Bongers, P. M. Castro, S. Engell, I. E. Grossmann, J. Hooker, C. Méndez, G. Sand, and J. Wassick (2014). Scope for industrial applications of production scheduling models and solution methods. *Computers & Chemical Engineering 62*, 161–193.

Sass, S., T. Faulwasser, D. E. Hollermann, C. D. Kappatou, D. Sauer, T. Schütz, D. Y. Shu, A. Bardow, L. Gröll, V. Hagenmeyer, D. Müller, and A. Mitsos (2020). Model compendium, data, and optimization benchmarks for sector-coupled energy systems. *Computers & Chemical Engineering 135*, 106760.

Skogestad, S., P. Lundström, and E. W. Jacobsen (1990). Selecting the best distillation control configuration. *AIChE Journal 36*(5), 753–764.

Skogestad, S. and M. Morari (1988). Understanding the dynamic behavior of distillation columns. *Industrial & Engineering Chemistry Research 27*(10), 1848–1862.

Zhang, Q. and I. E. Grossmann (2016). Planning and scheduling for industrial demand side management: Advances and challenges. In M. M. Martín (Ed.), *Alternative Energy Sources and Technologies*, Engineering, pp. 383–414. Switzerland: Springer.